Interlayer exchange coupling in Fe/Cr multilayers

L. Tsetseris, Byungchan Lee, and Yia-Chung Chang
Department of Physics and Materials Research Laboratory, University of Illinois at Urbana-Champaign, Urbana, Illinois 61801
(Received 3 June 1996)

We investigate the origin of the long-period oscillation of the interlayer exchange coupling in Fe/Cr trilayer systems. Within the stationary phase approximation the periods of the oscillations are associated with extremal vectors of the Fermi sphere of Cr. Using a realistic tight-binding model with spin-orbit interaction we calculate the coupling strength for each extremal vector based on the spin asymmetry of the reflection amplitude for a propagating state impinging from the Cr to Fe layer. We find that for the (001) and (110) growth directions the biggest coupling strength comes from the extremal vector centered at the ellipsoid N of the Fermi surface of Cr. [S0163-1829(97)10517-3]

I. INTRODUCTION

The magnetic properties of multilayer systems have been a subject of intensive study, particularly for the last decade. The initial observation that two ferromagnetic layers can be coupled antiferromagnetically, when separated by certain type of magnetic or nonmagnetic spacer (Grünberg *et al.*[1]), and the following discovery that this coupling possesses a damping oscillatory behavior (Parkin *et al.*[2]) stimulated a great deal of interest.[3] Moreover, because of the phenomenon of giant magnetoresistance (GMR),[4,5] these structures have become very promising candidates for applications in the magnetic recording industry.

The construction of ultrathin structures poses great challenges from the experimental point of view. The initial samples grown with sputtering displayed the characteristic oscillatory behavior, however, soon after the first measurements, the demand for strict control over stoichiometry and disorder made the growth of excellent epitaxial sandwiches or superlattices necessary. In the case of a sandwich, it is a common practice now that one uses a wedge geometry for the spacer layer.[6] In this way one can study the spacer thickness dependence of the interlayer exchange coupling (IEC) using only one sample.

From the theoretical perspective, the calculation of IEC has also attracted a lot of attention. Several different approaches to the problem have been suggested and used extensively. One can divide all these approaches into two major classes. One class consists of total-energy calculations, in which one calculates the difference in the total energy of the sample for the two important magnetization configurations (the magnetization of the ferromagnetic layers being parallel in one case, antiparallel in the other). Local-spin-density approximation (LSDA) (see for example Refs. 7,8) and semiempirical tight-binding (TB) methods[9,10] have been used for this purpose. The second class consists of various model calculations. In this we include the calculations based on the perturbative treatment of the Ruderman-Kittel-Kasuya-Yosida interaction,[11,12] an adapted Anderson (or sd-mixing) model,[13,14] and perhaps most importantly, we include all the various calculations of IEC that exploit the idea of quantum interference and quantum confinement in the spacer material.[15,16] The multiple reflections that the electrons experience at the spacer/magnetic layer interfaces bear an analogy to Fabry-Perot-like interferometry. Our own method belongs to this class. All the model calculations have certain approximations built in, and hence, one has to be aware that in some cases the accuracy of the results is limited. Nevertheless, the potential for numerical errors involved in these calculations is significantly smaller than in the total-energy calculations, particularly for large spacer thickness, and the computational effort is much less as well.

It is now widely accepted that the periods of the oscillations of IEC are given by the extremal vectors of the Fermi surface of the spacer material. In this paper we are going to study the IEC of Fe/Cr/Fe, so the spacer is Cr. Chromium has a complicated Fermi surface with a rich variety of spanning features. Therefore one would expect, in principle, a multiperiodic oscillation of IEC with respect to the Cr layer thickness. However, only two periods have been observed in the experiments so far. The short period is roughly equal to two monolayers (ML) of chromium and it is believed to be due to the nesting vector that gives rise to antiferromagnetism in Cr. The origin of the long period (measured to be somewhere between 15 and 18 Å) has been proven a more difficult problem.

We use an empirical TB method in order to calculate the coupling strengths associated with different periods. By using the ''force theorem,''[17] one can find the change in the density of states for the trilayer system with respect to the bulk case. Electrons with different spin see different effective potentials at the Fe/Cr interface, and consequently, the multiple reflections are sensitive to the magnetizations of the Fe layers being parallel or antiparallel. The base of the analytical work was developed in a series of papers by Bruno.[16] Stiles[18] and Slonczewski[19] also showed how one can calculate IEC based on the spin asymmetry of the reflection amplitudes. In more recent papers the method was applied with encouraging results in real systems.[20] We have used the same method as Lee and Chang used for Co/Cu/Co systems,[21] but with some modifications, in order to take care of the much more complicated Fermi surface of Cr. The main conclusion of our work is that the long-period oscillation originates from the extremal vector at the ellipsoid centered at point N of the Cr Fermi surface. This is true for both (001) and (110) growth directions. The result agrees with that obtained with

LDA calculations by Stiles.[22] We will also discuss its validity in view of the outcome of recent photoemission experiments.[23]

II. THEORETICAL MODEL

The Interlayer exchange coupling is defined as

$$J=\frac{\Omega_{\mathrm{F}}-\Omega_{\mathrm{AF}}}{2S}, \tag{1}$$

where Ω_{F} and Ω_{AF} are the grand canonical potentials for the ferromagnetic (F) and antiferromagnetic (AF) configurations and S is the area of the sample. In our case we consider a trilayer with semi-infinite Fe layers. The electrons are partially reflected at the interfaces of the Fe/Cr/Fe sandwich, and the change in the grand canonical potential is given by the force theorem (or the frozen potential approximation) as

$$\Delta\Omega_{\nu}=\frac{1}{\pi}\mathrm{Im}\sum_{\mathbf{k}_{\parallel}}\int_{-\infty}^{+\infty}d\epsilon f(\epsilon)\mathrm{Trln}(1-G_0T^{L,\nu}G_0T^{R,\nu}), \tag{2}$$

where ν labels the two configurations (F and AF), G_0 is the bulk Green's function of the spacer material, T is the T matrix, f is the Fermi-Dirac distribution, and L and R stand for the left and right interface, respectively. Tr denotes the trace over the z component of the wave vector and the spin index. The asymptotic form of IEC (for large thickness D of the Cr layer) is given in first order by the simple analytical result (see Ref. 21 for details)

$$J=\mathrm{Im}\sum_{\alpha}\sum_{ij}\frac{\hbar u_{ij}^{\alpha}\kappa_{ij}^{\alpha}}{4\pi^2D^2}\Delta R_{ij}^{\alpha}e^{i(q_{ij}^{\alpha}D+\phi_{ij}^{\alpha})}F_{ij}^{\alpha}(D,T)\,\theta_{ij}, \tag{3}$$

where

$$\Delta R_{ij}^{\alpha}=\sum_{\sigma\sigma'}(r_{Rij}^{\sigma\sigma'F}r_{Lji}^{\sigma'\sigma F}-r_{Rij}^{\sigma\sigma'F}r_{Lji}^{\sigma'\sigma AF}), \tag{4}$$

$$F_{ij}^{\alpha}(D,T)=\frac{2\pi k_BTD/\hbar u_{ij}^{\alpha}}{\sinh(2\pi k_BTD/\hbar u_{ij}^{\alpha})}, \tag{5}$$

and

$$\frac{1}{u_{ij}^{\alpha}}=\frac{1}{u_i^{\alpha}}-\frac{1}{u_j^{\alpha}}. \tag{6}$$

In Eq. (3), $q_{ij}^{\alpha}=k_j^{\alpha}-k_i^{\alpha}$ is an extremal vector of the Fermi surface of Cr parallel to the growth direction (which is taken to be the $\hat{z}$ direction). The superscript α labels different $\mathbf{k}_{\parallel}^{\alpha}$, that is the in-plane component of the wave vector. k_i^{α} and k_j^{α} are the z components of the wave vector of the incident (reflected) and reflected (incident) electron for the right (left) interface, and u_i^{α} is the group velocity at a point $(\mathbf{k}_{\parallel}^{\alpha},k_i^{\alpha})$ of the Fermi sphere. The index σ labels the two spin mixed states that are degenerate at each $(\mathbf{k}_{\parallel}^{\alpha},k_i^{\alpha})$ (Kramers degeneracy). The reflection amplitude from a state (k_i^{α},σ) to a state (k_j^{α},σ') is denoted by $r_{Iij}^{\sigma\sigma'\nu}$ (where $I=L,R$ labels the interfaces). κ_{ij}^{α} is related to the curvature radii at the two endpoints of q_{ij}^{α},

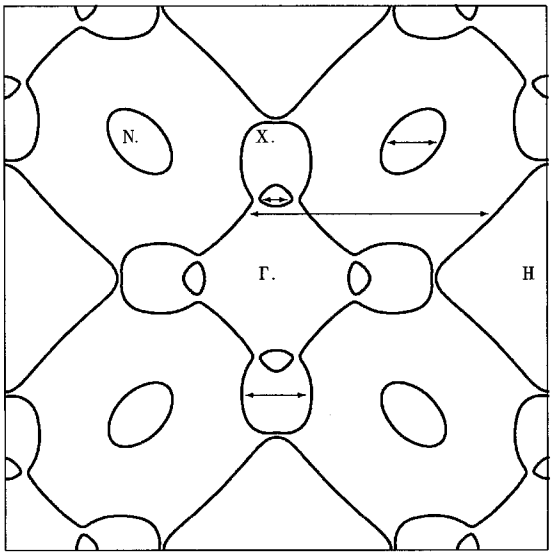

FIG. 1. (100) cross section of Cr Fermi surface.

$$\kappa_{ij}^{\alpha}=\left[\sqrt{\left|\frac{\partial^2q_{ij}^{\alpha}}{\partial k_x^2}\frac{\partial^2q_{ij}^{\alpha}}{\partial k_y^2}-\left(\frac{\partial^2q_{ij}^{\alpha}}{\partial k_x\partial k_y}\right)^2\right|}\right]^{-1}. \tag{7}$$

The product

$$G_{ij}^{\alpha}=\frac{\hbar}{2\pi^2}u_{ij}^{\alpha}\kappa_{ij}^{\alpha} \tag{8}$$

is called the geometrical weight of the extremal vector q_{ij}^{α}. D is the thickness of the Cr layer, θ_{ij} is a constraint function, which is 1 for extremal vectors and 0 otherwise. The phase factor $\phi_{ij}^{\alpha}=0$, $\pi/2$, and π for maximum, saddle, and minimum extremal points, respectively. We perform the calculation at zero temperature, so $F_{ij}^{\alpha}(D,T)=1$. For finite temperatures $F_{ij}^{\alpha}(D,T)$ is less than 1, if the spacer is metallic.[16]

The reflection amplitude factor ΔR_{ij}^{α} depends explicitly on the reflection amplitudes, which, as we mentioned above, are calculated from an empirical TB model with s, p^3, and d^5 orbitals. Because of the sandwich geometry one needs to include, not only the propagating Bloch solutions, but also the evanescent states, i.e., the states with complex wave vectors. The reflection amplitudes are calculated for a heterostructure geometry, with semi-infinite slabs of Fe and Cr on the right and left side of the their interface. The TB parameters at the interface are calculated as an average of the Fe and Cr parameters, an approximation which is reliable when, as in this case, the two interface materials have similar TB overlap integrals. The details of the method can be found in Ref. 24. For Cr, the spin-orbit coupling is significant only for the so-called lens area and at the point across the ΓH line where the electron surface almost touches the hole surface (see Fig. 1). For all other vectors the spin-orbit interaction does not play an important role, the spin is approximately a good quantum number, and one finds that

$$\Delta R_{ij}^{\alpha}\approx(r_{Rij}^{\alpha+}-r_{Rij}^{\alpha-})(r_{Lji}^{\alpha+}-r_{Lji}^{\alpha-}), \tag{9}$$

where the superscript $+$ $(-)$ denotes majority (minority) spin electron.

TABLE I. Results for (001) orientation.

Vector	$\mathbf{k}_{\parallel}$ $[2\pi/a]$	λ (Å)	G^{α} (meV)	$\lvert\Delta R\rvert$	J^{α} (mJ/m^2)
	(0,0)	5.56	8.48	1.01	0.68
	(0,0)	9.20	160.12	9.0×10^{-5}	2.3×10^{-3}
	(0,0)	4.18	1.87	0.88	0.13
	(0,0)	33.65	3.40	6.9×10^{-3}	3.8×10−3
$\overline{V_n}$	(0,0.25)	3.12	146.88	0.40	37.99
$\overline{L_1}$	(0,0.29)	20.85	1.00	1.7×10^{-3}	5.3×10^{-4}
$\overline{L_2}$	(0,0.29)	17.77	1.39	0.41	0.18
$\overline{X}$	(0,0.42)	11.21	36.99	0.24	2.81
$\overline{N_1}$	(0.0,0.5)	13.77	24.06	1.03	7.94
$\overline{N_2}$	(0.5,0.5)	10.38	10.40	0.63	1.03
	(0,1.0)	3.42	6.33	0.65	0.33

III. Fe/Cr/Fe SANDWICHES

As we pointed out in Sec. I, the Fe/Cr/Fe case has been a difficult one for the calculation of IEC, and this is mainly because of the complicated Fermi surface of Cr. For our own TB calculations we have used the parameters from Ref. 25. These parameters do not include any relativistic effects, and particularly spin-orbit coupling. We have included spin-orbit coupling with its characteristic parameter $\xi=2.84$ mRy taken from Ref. 26. This value agrees well also with the value found in Ref. 17. The (100) cross section of the Fermi surface, that we obtained, is shown in Fig. 1. In this figure we used a slightly larger parameter ξ, so that the effects of the spin-orbit interaction become easier to see. The Fermi surface we obtained (with the correct ξ) agrees very well qualitatively, and in most cases quantitatively, with the ones obtained from experiments and other more involved band-structure calculations (see for example Ref. 27). The inclusion of spin-orbit coupling affects significantly the area around the lens vector, as we mentioned before. One needs to take this effect into consideration, because the period related to this vector is very close to the long period of the oscillations of IEC.

Our results are summarized in Tables I and II for the two growth directions that we have studied. In the tables, $c=a/2, a/\sqrt{2}$ is the distance between two Cr layers for (001) and (110) orientation, respectively ($a=2.88$ Å is the Cr lattice constant), and λ's are the periods that we found. In the last column we give the coupling strength

$$J_{ij}^{\alpha}=\frac{G_{ij}^{\alpha}n|\Delta R|}{2D^2} \tag{10}$$

associated with each vector q_{ij}^{α}. G_{ij}^{α} is the geometrical weight and n is the number of equivalent extremal vectors in the first Brillouin zone. For the thickness D we take a typical value of 10 Å. One can see that $|\Delta R|$ and G_{ij}^{α} vary significantly for different extremal vectors, and therefore, the overall coupling strength is not negligible only for very few vectors. In the next two subsections we shall discuss the analyses for (001) and (110) orientations separately.

A. (001) orientation

In Fig. 1, we give the (100) cross section of the Cr Fermi sphere. The wave vectors are measured in $2\pi/a$. We have marked some extremal vectors, which, according to the theory, are candidates for the observed periods of the oscillations of IEC. Four vectors are of particular importance. One is the vector ($\overline{N_1}$) at the ellipsoid pocket at $\underline{N}$. Two other special vectors are the one spanning the lens ($\overline{L_1}$) and the one just outside the lens ($\overline{L_2}$). Finally, we have the nesting vector ($\overline{V_n}$), which connects two almost parallel lines, one from the electron octahedron around point Γ, and the other from the hole octahedron around point H.

TABLE II. Results for (110) orientation.

Vector	$\mathbf{k}_{\parallel}$ $[2\pi/a]$	λ (Å)	G^{α} (meV)	$\lvert\Delta R\rvert$	J^{α} (mJ/m^2)
	(0,0)	5.86	18.78	0.58	0.86
$\overline{L_1'}$	(0,0.29)	21.26	1.37	0.97	0.21
$\overline{L_2'}$	(0,0.29)	17.87	1.57	1.11	0.28
$\overline{L_3'}$	(0.23,0)	29.68	3.86	6.0×10^{-3}	3.6×10^{-3}
$\overline{X'}$	(0,0.44)	9.42	6.01	0.93	0.89
$\overline{N_1'}$	(0.71,0)	16.46	38.45	1.51	4.65
$\overline{N_2'}$	(0.35,0.50)	12.12	15.41	0.24	1.17
$\overline{N_3'}$	(0.71,1.0)	10.04	7.67	0.25	0.15
	(0.3,0.0)	9.73	12.93	0.07	0.30
$\overline{S'}$	(0,1.0)	4.70	43.31	0.59	2.02

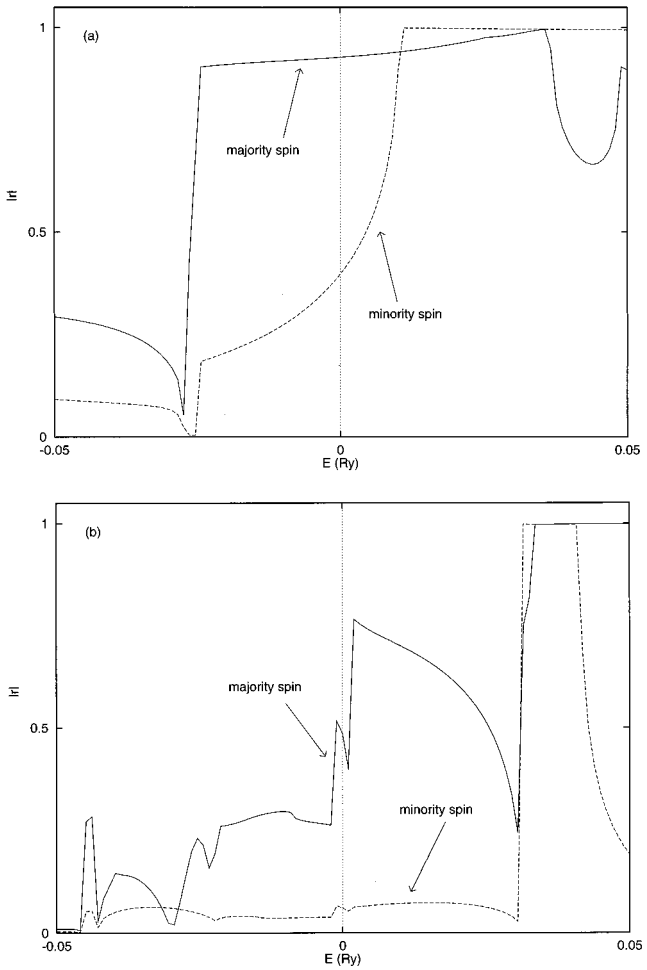

FIG. 2. Moduli of the reflection amplitudes vs energy for (001) orientation. (a) $\mathbf{k}_\parallel=(0,0.5)2\pi/a$, (b) $\mathbf{k}_\parallel=(0,0.42)2\pi/a$ (Fermi energy is aligned to be zero).

For the extremal vector $\overline{N_1}$, both G_{ij}^{α} and $|\Delta R|$ are big, and hence, the coupling strength is large (7.94 mJ/m^2). The next closest amplitude is 2.80 mJ/m^2, for the extremal vector X that spans the electron ball at point X $[\mathbf{k}_\parallel=(0,0.42)2\pi/a]$. This is still 2.83 times smaller than the ellipsoid contribution. All the other amplitudes, with the exception of the nesting vector, are, approximately, at least one order of magnitude smaller. In Figs. 2(a) and 2(b), we present the behavior of the modulus of the reflection amplitude $|r^+|$ $(|r^-|)$ of the majority (minority) spin electron as a function of the energy for $\mathbf{k}_\parallel=(0,0.5)2\pi/a$ and $\mathbf{k}_\parallel=(0,0.42)2\pi/a$. For these $\mathbf{k}_\parallel$'s, the spin-orbit coupling is not very important and $|\Delta R|$ is given explicitly by the square of the difference of r^+ and r^-. These two complex numbers mirror the match or the mismatch of the bands of Cr and Fe at the Fermi level and at this particular $\mathbf{k}_\parallel$. The band structure along k_z at $\mathbf{k}_\parallel=(0,0.5)2\pi/a$ for Cr and Fe is given in Fig. 3. For both Fe and Cr the Fermi level is aligned to be at zero energy.

One can see from Fig. 2(b) $[\mathbf{k}_\parallel=(0,0.42)2\pi/a]$ that $|r^+|$ changes very rapidly around the Fermi energy. This means that the stationary phase approximation is not very well satisfied for this $\mathbf{k}_\parallel$. Therefore, the result for the coupling strength for X is not very reliable. For $\overline{N_1}$ on the other hand, the variation of $|r^+|$ and $|r^-|$ around the Fermi level is smooth. The majority electrons of the ellipsoid are reflected strongly at the interface, because they have to transmit from a Cr sp band to an Fe d band (see Fig. 3). The minority electrons have smaller reflection amplitude $|r^-|$ because the related Fe band at the Fermi level is of the same character as the Cr band. As soon as the energy is raised by ≈ 0.01 Ry, the Fermi level minority band of Fe changes symmetry, and the minority electrons become completely confined at the Cr layer.

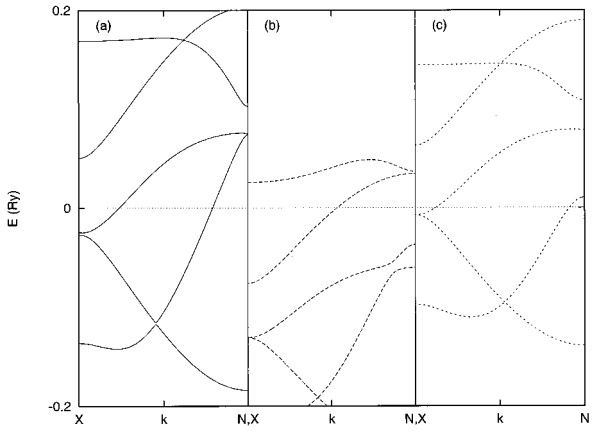

FIG. 3. Band structure along line XN $[\mathbf{k}_\parallel=(0,0.5)2\pi/a]$ for (a) Cr, (b) majority Fe, and (c) minority Fe.

Our calculations give a period of 13.77 Å for $\overline{N_1}$. This period is slightly smaller than the experimental value for the long-period oscillation, which is somewhere between 14 and 18 Å (see for example Refs. 2,6,28). For this same vector, the de Haas–van Alphen experiments[29] give a period of 15.97 Å, which is within the experimental uncertainty. The fact that our calculated period is smaller than the experimental one is not really a crucial mistake for the calculation of the coupling strength, which is the main focus of our work. One can actually easily tune the tight-binding parameters so that one gets an ellipsoid period closer to the de Haas–van Alphen experiments. However this tuning of the parameters would not affect essentially the coupling strength, which depends on the symmetry of the states that are involved in the reflection and transmission of the electrons, and not on the accurate size of some parts of the Fermi sphere. With a satisfactory period and coupling strength (as we will argue in the Sec. IV), the vector N_1 is the best candidate for the origin of the long-period oscillations of IEC, at least within the reflection amplitude approximation.

The very existence of the lens is due to the spin-orbit coupling that we have included for Cr. In the case of vanishing spin-orbit parameter ξ the lens touches the outside surface and there is no extremal vector at this point. With $\xi=2.84$ mRy we obtained two extremal vectors $\overline{L_1}$ and $\overline{L_2}$ at $\mathbf{k}_\parallel=(0,0.29)2\pi/a$, which have periods 20.85 and 17.77 Å, respectively. For both vectors, the factor $|\Delta R|$ is not small, but in contrast to the nesting vector case, the curvature radius factor κ_{ij}^{α} is very small. Thus the overall contribution to the coupling is almost negligible. This is a somehow unwelcome result because the periods of $\overline{L_1}$ and $\overline{L_2}$ are very close to the experimental one. However, it is a result that one would

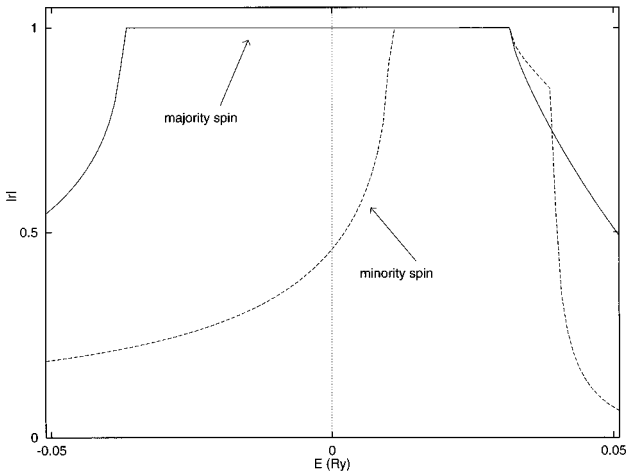

FIG. 4. Moduli of the reflection amplitudes vs energy for (110) orientation and $\mathbf{k}_{\parallel}=(0.71,0)2\pi/a$ (Fermi energy is aligned to be zero).

anticipate from qualitative reasoning alone, since the phase space associated with the lens is small, as has been stressed by other authors previously.[8]

The nesting vector $\overline{V_n}$ corresponds to a period of about 3.12 Å. This is about 2.17 ML of Cr and agrees very well with previous results. For this vector, the geometrical weight is very big (approximately at least an order of magnitude bigger than most of the other G_{ij}^{α}'s presented in Table I). This is as expected qualitatively, because the nesting feature (nearly parallel lines) leads to very large value for κ_{ij}^{α}. Since the reflection factor $|\Delta R|$ is not very small, the overall coupling strength associated with $\overline{V_n}$ is large (37.99 mJ/m^2). Although this number is too big compared to experimental strengths, the result agrees with the experiment qualitatively, since it renders $\overline{V_n}$ the best candidate for the short-period oscillations [for which the period is measured to be 2.1 ML (Refs. 6 and 28)]. Nevertheless, one has to acknowledge that the nesting feature requires a treatment that goes beyond the stationary phase approximation used in our calculations. Specifically the replacement of the Fermi-surface sheets by parabolas is questionable for this case, and one should perform an explicit numerical integration over $\mathbf{k}_{\parallel}$ for this particular area of the Fermi sphere. Moreover, the coupling strength of the short-period oscillations is very sensitive to roughness, as will be discussed in Sec. IV.

B. (110) orientation

In Table II we give the results of the calculation for the (110) orientation. Again, as in the (001) case, one can find, among others, extremal vectors that span the lens ($\overline{L_1'}$, $\overline{L_2'}$, and $\underline{L_3'}$) and vectors (for example $\overline{N_1'}$) at the N ellipsoid. As we can see in this case, the most important contribution to the coupling is made by $\overline{N_1'}$. Its period and strength are found to be 16.46 Å [the experimental period is $\approx$ 18 Å (Refs. 2 and 30)], and 4.65 mJ/m^2, respectively. In Fig. 4, we give the moduli of the reflection amplitudes $|r^+|$ and $|r^-|$ as a function of energy. The majority electrons are strongly confined in the spacer, whereas the minority electrons are only partially reflected at the interface. The change of $|r^+|$ and $|r^-|$ around the Fermi level is slow enough that the stationary phase approximation is reliable.

The lens vectors $\overline{L_1'}$, $\overline{L_2'}$, and $\underline{L_3'}$ have again small κ_{ij}^{α}, and small overall coupling strengths. A significant contribution is made from the vector $\overline{X'}$ at $\mathbf{k}_{\parallel}=(0,0.44)2\pi/a$. Note that we have used new x',y',z' axes so that $\hat{z}'$ is the growth direction. Another ellipsoid vector at $\mathbf{k}_{\parallel}=(0.35,0.50)2\pi/a$ has also large J_{ij}^{α}. Anyway, these two J_{ij}^{α}'s (0.89 mJ/m^2 and 1.17 mJ/m^2) are five and four times smaller than that of $\overline{N_1'}$. Therefore, the origin of the long-period oscillations is attributed again to an ellipsoid spanning vector. There is also a non-negligible strength associated with short-period oscillations. This is for $\mathbf{k}_{\parallel}=(0.0,1.0)2\pi/a$, with a period of 4.70 Å and a strength of 2.02 mJ/m^2. To the best of our knowledge, no short period has been reported so far for the (110) orientation.

IV. DISCUSSION OF RESULTS

As we stressed in the previous sections, the two most important issues that one has to address for IEC are the period of the oscillation and its magnitude. For the three cases of (001), (110), and (211) orientation, the experimental data give a similar period. The common period is in favor of the argument that the large-wavelength oscillations are originated from a relatively isotropic part of the Cr Fermi surface. As we saw above, our calculations agree with that, since the two vectors $\overline{N_1}$ and $\overline{N_1'}$ are extremal vectors of the ellipsoid centered at N, which is fairly isotropic. The size of the ellipsoid, as we calculated it in the (110) case (period 16.46 Å) or as it can be calculated from de Haas–van Alphen experiments for the (001) case (period 15.97 Å), is in good agreement with the observed period.

The measured coupling strengths for the (001) orientation vary from 0.6 mJ/m^2 to 1.6 mJ/m^2 for thicknesses between 4 and 8 ML.[28,31,32] Our own result is 7.94 mJ/m^2 for $D=10$ Å, if we use Eq. (10), whereas if we use Eq. (3), we find that the first antiferromagnetic peak strength is 14.45 mJ/m^2 for $D=6.7$ Å. These numbers are about ten times the experimental ones. Previous total-energy calculations (see Sec. 2.2 in Ref. 3) predicted larger amplitudes (up to 100 bigger than the experiment), so our result is an improvement. In a most recent first-principles calculation, Stiles[22] also attributed the origin of the long-period oscillations to $\overline{N_1}$ and $\overline{N_1'}$. His calculated coupling strengths for these vectors are 5.7 mJ/m^2 and 3.2 mJ/m^2. Both numbers are in good agreement with ours.

The discrepancy with the experiment can be remedied if the interface roughness is taken into account. The coupling strength in realistic samples decreases mostly because of the interface roughness. In the experiment, the Fe/Cr interfaces are not ideally flat, but they possess steps, that lead to a random growth front of the Cr spacer. One can deduce from the experimental data that early results, obtained from rough samples grown with sputtering, gave smaller strengths compared to more recent ones from smooth epitaxial films. Our calculation can be modified in two ways in order to include the effects of interface roughness. First, we can average the amplitude of IEC over the variable thickness of the film. As is shown in Refs. 12 and 13, this can be done by convoluting

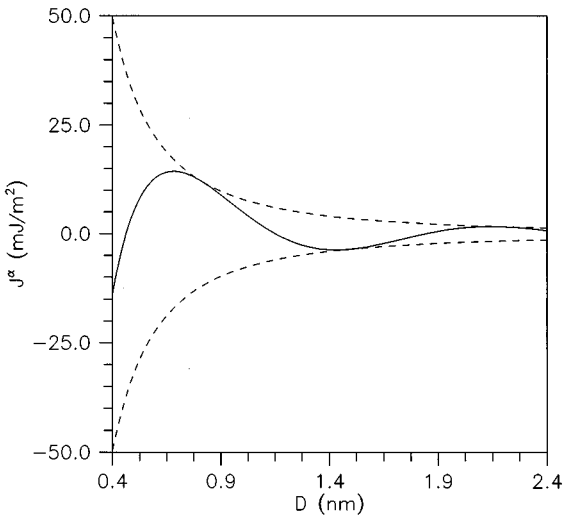

FIG. 5. Coupling strength J^α vs thickness D, as calculated from (a) Eq. (3) (solid line), (b) Eq. (10) (dashed line).

the coupling strength $J(t)$ for a certain thickness t with a distribution (constant or Gaussian) over t fluctuations. Consequently, the new coupling is

$$J_{\text{rough}}(D)=\sum_t P(D,t)J(t), \tag{11}$$

where D is the average thickness. Second, because of the roughness, the in-plane component of the wave vector is no longer a good quantum number. A certain $\mathbf{k}_\parallel$ state can be reflected to a range of other $\mathbf{k}_\parallel$'s states around it, and this leads to a decrease of the coupling, or even to complete sweep of the oscillations, if the period is short. Therefore, if the sample is not prepared to be smooth, the 2.2-ML period associated with the nesting vector will not be observed. This has been verified experimentally.[2,6] Interface roughness may also be responsible for the lack of the period of 4.70 Å that we found in the (110) case. Apart from roughness, other disorder effects, like misfit dislocations and strain,[12] also can affect IEC in the same way. These effects however do not play any significant role in Fe/Cr multilayers because of the excellent match of the lattice constants (2.88 Å for Cr, 2.87 Å for Fe).

The number that we give as the amplitude is really an upper bound of the actual value, since we are taking the absolute value of the complex number $|\Delta R|$. This is demonstrated in Fig. 5, which shows J_{ij}^α vs thickness D as calculated from Eqs. (3) and (10) for the spanning vector N_1. We use $|\Delta R|$ to estimate the strength of IEC, because there is a certain phase arbitrariness in the calculation. The main source for this is the finite thickness of the Fe layers, which is not taken into account in our calculation. It has been predicted from theory[16,33] and verified experimentally,[34] that IEC exhibits oscillations, not only as a function of Cr thickness, but also as one varies the thickness of the Fe layers. This means of course that the antiferromagnetic peaks occur at different D for different Fe widths, and so one needs to use the right D in each case. Moreover, for finite thickness, quantum well states are expected to be formed also in the magnetic layers and hence the coupling strength will be affected as well. Finally, we must point out once more that our approximations do not hold for very thin multilayers, and hence the initial phase is pretty arbitrary.

Our results indicate that the nesting vector of the ellipsoid is a favorite candidate for the long period oscillations. However, other candidates have been proposed in the literature as well. Early on, it was realized that the nesting vector can be responsible, not only for the small, but also for the large wavelength oscillations. Because of the discreteness of the thickness D, a short period can give rise to an effective long period as a higher harmonic. The phenomenon is called aliasing and one gets for the second harmonic a period $\lambda'=\lambda/(\lambda-2)$ ML. For $\lambda\approx 2.2$ ML the effective period is indeed large. However, careful measurements of the large period by Pierce *et al.*[6] gave an effective period $\lambda'=20.05$ ML, much bigger than the observed period which is between 10 and 12 ML. Moreover, the fact that the period seems to be independent of the orientation is not in favor of the aliasing scenario. Of course from the theoretical point of view, a conclusive analysis would be to calculate the coupling strength for the second harmonic and see if it is significant. The nesting vector though is a difficult case, as we mentioned in Sec. III. If the coupling strength for the second harmonic turns out to be comparable to the one of the vector N_1, then the superposition of the two oscillations will lead to new features in the overall IEC, particularly it will raise its period and also decrease its amplitude.

Two other candidates for the long-period coupling are the lens vectors L_1 and L_2. In a recent paper, Li *et al.*[23] have studied the confinement of electrons in the spacer using angle-resolved photoemission. They found substantial confinement for states with $\mathbf{k}_\parallel$ in the vicinity of the lens. From this they concluded that the lens is the k-space origin of the long-period oscillations. From our calculations we have found that the confinement at the lens area is big enough that one could detect quantum well states for this $\mathbf{k}_\parallel$ (the magnitude of both r^+ and r^- in the ferromagnetic configuration is ≈ 0.5). However, the confinement is much stronger at the ellipsoid as one can see in Fig. 2(a). Hence it would be useful to get more data for this k-space area. The confinement is one important factor for IEC, but there are also other factors that affect the amplitude of the oscillation. Most important one is the spin asymmetry of the reflection amplitude (as a difference of two complex numbers), and not individual magnitude by itself. The geometrical weight of the vector is a crucial factor as well, at least within the stationary phase approximation. For the lens vectors, G_{ij}^α's are very small.

Although our result seems to be in fairly good agreement with the experiment, one should stress the point that the reflection amplitude approximation is the first step towards the reliable determination of IEC. Total-energy methods can take on the predictions of this method and improve the calculation. However, given the numerical problems that the total-energy methods suffer, especially in the case of Cr-based multilayer systems, this first step gives a very valuable, simplified and physically transparent approach to the problem in hand, and a very useful checkpoint of the asymptotic behavior of IEC for future, more ambitious calculations.

V. SUMMARY

By using an empirical TB method (including s, p^3, and d^5 orbitals) and including the spin-orbit interaction, we have calculated the reflection amplitudes and transmission coefficients for an Fe/Cr/Fe sandwich structure. Based on the spin asymmetry of these quantities and the geometrical weight of the extremal vectors of the Cr Fermi surface, we have obtained the coupling strengths associated with each vector. For both (001) and (110) growth direction, the origin of the long-period oscillations of the exchange coupling is attributed to extremal vectors of the ellipsoid centered at point N. The period agrees satisfactorily with the observed value. The coupling strength is roughly an order of magnitude bigger than the experimental one, but the inclusion of interface roughness in the calculation can improve the agreement substantially. Although the attribution of the long-period coupling to the aliasing effect of the nesting vector faces several opposing arguments, one should try to calculate more carefully the coupling strength of the second harmonic of this vector. Within the approximations that we have used, all the other candidates for the long period (and in particular the lens vectors) have been found to have a small to negligible contribution to the overall coupling.

ACKNOWLEDGMENTS

This work was supported by the University of Illinois research board and the University of Illinois Materials Research Laboratory through Contract No. NSF/DMR-89-20538.

[1] P. Grünberg, R. Schreiber, Y. Pang, M. B. Brodsky, and H. Sowers, Phys. Rev. Lett. **57**, 2442 (1986).
[2] S. S. P. Parkin, N. More, and K. P. Roche, Phys. Rev. Lett. **64**, 2304 (1990).
[3] For a review of interlayer exchange coupling, see *Ultrathin Magnetic Structures II*, edited by B. Heinrich and J. A. C. Bland (Springer-Verlag, Berlin, 1994), Chap. 2.
[4] M. N. Baibich, J. M. Broto, A. Fert, F. Nguyen Van Dau, F. Petroff, P. Etienne, G. Creuzet, A. Friederich, and J. Chazelas, Phys. Rev. Lett. **61**, 2472 (1988); G. Binasch, P. Grünberg, F. Saurenbach, and W. Zinn, Phys. Rev. B **39**, 4828 (1989).
[5] For a review of GMR, see P. M. Levy, Solid State Phys. **47**, 367 (1994).
[6] J. Unguris, R. J. Celotta, and D. T. Pierce, Phys. Rev. Lett. **67**, 140 (1991); R. J. Celotta, J. Unguris, and D. T. Pierce, J. Appl. Phys. **75**, 6452 (1994); D. T. Pierce, J. A. Stroscio, J. Unguris, and R. J. Celotta, Phys. Rev. B **49**, 14 564 (1994).
[7] F. Herman, J. Sticht, and M. van Schilfgaarde, J. Appl. Phys. **69**, 4783 (1991); M. van Schilfgaarde, F. Herman, S. S. P. Parkin, and J. Kudrnovský, Phys. Rev. Lett. **74**, 4063 (1995); S. Mirbt, H. L. Skriver, M. Alden, and B. Johansson, Solid State Commun. **88**, 331 (1993).
[8] M. van Schilfgaarde and F. Herman, Phys. Rev. Lett. **71**, 1923 (1993).
[9] H. Hasegawa, Phys. Rev. B **42**, 2368 (1990).
[10] D. Stoeffler and F. Gautier, Prog. Theor. Phys. Suppl. **101**, 139 (1990).
[11] Y. Yafet, Phys. Rev. B **36**, 3948 (1987); W. Baltensberger and J. S. Helman, Appl. Phys. Lett. **57**, 2954 (1990).
[12] P. Bruno and C. Chappert, Phys. Rev. B **46**, 261 (1992).
[13] Y. Wang, P. M. Levy, and J. L. Fry, Phys. Rev. Lett. **65**, 2732 (1990).
[14] Z. P. Shi, P. M. Levy, and J. L. Fry, Phys. Rev. Lett. **69**, 3678 (1992); P. Bruno, J. Magn. Magn. Mater. **116**, L13 (1992).
[15] D. M. Edwards, J. Mathon, R. B. Muniz, and M. S. Phan, Phys. Rev. Lett. **67**, 493 (1991); D. M. Edwards and J. Mathon, J. Magn. Magn. Mater. **93**, 85 (1991).
[16] P. Bruno, J. Magn. Magn. Mater. **121**, 248 (1993); Europhys. Lett. **23**, 615 (1993); Phys. Rev. B **49**, 13 231 (1994).
[17] A. R. Mackintosh and O. K. Andersen, in *Electrons at the Fermi Surface*, edited by M. Springford (Cambridge University Press, Cambridge, England, 1980).
[18] M. D. Stiles, Phys. Rev. B **48**, 7238 (1993).
[19] J. C. Slonczewski, J. Magn. Magn. Mater. **150**, 13 (1995).
[20] P. Bruno, Phys. Rev. B **52**, 411 (1995); M. D. Stiles, J. Appl. Phys. **79**, 5805 (1996).
[21] B. Lee and Y.-C. Chang, Phys. Rev. B **52**, 3499 (1995).
[22] M. D. Stiles, Bull. Am. Phys. Soc. **41**, 36 (1996); Phys. Rev. B **54**, 14 679 (1996).
[23] D. Li, J. Pearson, S. D. Bader, E. Vescovo, D.-J. Huang, P. D. Johnson, and B. Heinrich, Phys. Rev. Lett. **78**, 1154 (1997).
[24] Y.-C. Chang and J. N. Schulman, Phys. Rev. B **25**, 3975 (1982).
[25] D. A. Papaconstantopoulos, *Handbook of the Band Structure of Elemental Solids* (Plenum, New York, 1986).
[26] F. Herman and S. Skillman, *Atomic Structure Calculations* (Prentice-Hall, New Jersey, 1963).
[27] E. Fawcett, Rev. Mod. Phys. **60**, 209 (1988), and references therein.
[28] S. T. Purcell, W. Folkerts, M. T. Johnson, N. W. E. McGee, K. Jager, W. B. Zeper, W. Hoving, and P. Grünberg, Phys. Rev. Lett. **67**, 903 (1991); S. Demokritov, J. A. Wolf, and P. Grünberg, Europhys. Lett. **15**, 881 (1991); P. Grünberg, S. Demokritov, A. Fuss, R. Schreiber, J. A. Wolf, and S. T. Purcell, J. Magn. Magn. Mater. **104-107**, 1734 (1992).
[29] J. E. Graebner and J. A. Marcus, Phys. Rev. **175**, 659 (1968). This work is for AF Cr.
[30] S. S. P. Parkin, Phys. Rev. Lett. **67**, 3598 (1991).
[31] E. E. Fullerton, M. J. Conover, J. E. Mattson, C. H. Sowers, and S. D. Bader, Phys. Rev. B **48**, 15 755 (1993).
[32] A. Fert, P. Grünberg, A. Barthélémy, F. Petroff, and W. Zinn, J. Magn. Magn. Mater. **140-144**, 1 (1995).
[33] J. Barnaś, J. Magn. Magn. Mater. **111**, L215 (1992).
[34] S. N. Okuno and K. Inomata, Phys. Rev. Lett. **72**, 1553 (1994).